Eur J Nucl Med Mol Imaging (2009) 36:1639–1650
DOI 10.1007/s00259-009-1156-3

ORIGINAL ARTICLE

Advancement in PET quantification using 3D-OP-OSEM point spread function reconstruction with the HRRT

Andrea Varrone · Nils Sjöholm · Lars Eriksson · Balazs Gulyás · Christer Halldin · Lars Farde

Received: 30 December 2008 / Accepted: 17 April 2009 / Published online: 13 May 2009

Abstract
Purpose Image reconstruction including the modelling of the point spread function (PSF) is an approach improving the resolution of the PET images. This study assessed the quantitative improvements provided by the implementation of the PSF modelling in the reconstruction of the PET data using the High Resolution Research Tomograph (HRRT).
Methods Measurements were performed on the NEMA-IEC/2001 (Image Quality) phantom for image quality and on an anthropomorphic brain phantom (STEPBRAIN). PSF reconstruction was also applied to PET measurements in two cynomolgus monkeys examined with [^{18}F]FE-PE2I (dopamine transporter) and with [^{11}C]MNPA (D_2 receptor), and in one human subject examined with [^{11}C]raclopride (D_2 receptor).
Results PSF reconstruction increased the recovery coefficient (RC) in the NEMA phantom by 11–40% and the grey to white matter ratio in the STEPBRAIN phantom by 17%. PSF reconstruction increased binding potential (BP_{ND}) in the striatum and midbrain by 14 and 18% in the [^{18}F]FE-PE2I study, and striatal BP_{ND} by 6 and 10% in the [^{11}C]MNPA and [^{11}C]raclopride studies.
Conclusion PSF reconstruction improved quantification by increasing the RC and thus reducing the partial volume effect. This method provides improved conditions for PET quantification in clinical studies with the HRRT system, particularly when targeting receptor populations in small brain structures.

Keywords Resolution · Modelling · Small brain nuclei · Partial volume effect

A. Varrone (✉) · N. Sjöholm · L. Eriksson · B. Gulyás · C. Halldin · L. Farde
Karolinska Institutet, Department of Clinical Neuroscience, Psychiatry Section and Stockholm Brain Institute, R5:02, Karolinska Hospital, 17176 Stockholm, Sweden
e-mail: andrea.varrone@ki.se

L. Eriksson
Siemens Molecular Imaging, Knoxville, TN, USA

L. Eriksson
Department of Physics, University of Stockholm, Stockholm, Sweden

Introduction

The performance of positron emission tomography (PET) has improved considerably since the technique was introduced in the 1970s. The implementation of detector crystals with high stopping power, high light output and fast decay, together with improved ring design and electronics has led to major advancements. The High Resolution Research Tomograph (HRRT) (Siemens Molecular Imaging) is a PET system with high spatial resolution designed for imaging of the human brain. The HRRT system has a spatial resolution of approximately 2.5 mm in the centre and 3.5 mm at 14 cm off-centre full-width at half-maximum (FWHM) [1] and is primarily used for studies of brain metabolism and radioligand binding to neuroreceptors [2–5]. PET imaging with the HRRT would provide better quantification of neuroreceptors in the human brain, particularly for those monoamine transporter populations that are highly expressed in small brain nuclei, such as the locus coeruleus or the substantia nigra.

Along with improvement of hardware, software development for more accurate image reconstruction and quantification has been of great importance in the field of molecular imaging. Image reconstruction including modelling of the scanners' point spread function (PSF) in the system matrix is an approach improving the spatial resolution of the PET

images [6, 7]. This approach has been validated and implemented in new whole-body PET/CT systems, such as the Siemens Biograph (Hi-Rez) scanner, in which it has been shown that PSF reconstruction improves the resolution and also provides a more uniform resolution across the field of view [6].

Partial volume effect (PVE) is a main factor contributing to reduced accuracy in the quantification of the PET signal [8–11] in particular in small brain structures. The combination of high-resolution imaging with the HRRT and the improved spatial resolution using PSF reconstruction may provide a means for improving the quantification and reducing the PVE in neuroreceptor PET studies. Indeed, PSF reconstruction has recently been implemented and validated in the HRRT system and applied to human [^{11}C]PE2I PET measurements, showing approximately 20–25% increase in dopamine transporter binding potential in the striatum as compared with the conventional iterative reconstruction method [7].

The reconstruction algorithm that includes modelling of the PSF [7] has been implemented in the HRRT system at the Karolinska Institutet PET Centre. In this study we examined the effects of the improved resolution of the HRRT images obtained with PSF reconstruction on the recovery coefficient (RC), the time-activity curves (TACs) in target and background regions and the quantitative outcome measure, the binding potential, of dopamine transporter or dopamine D_2 receptor density. The quantitative performance of PSF reconstruction was compared with the one from the standard reconstruction algorithm. This comparative analysis was based on phantom measurements as well as on studies of dopaminergic markers in two non-human primates and in one human subject.

Material and methods

The HRRT system

The HRRT system (Siemens Molecular Imaging) was installed in 2007 at the PET Centre, Karolinska University Hospital, Solna, Sweden. The system consists of eight panel detectors with an octagonal configuration. Each panel has 9*13 phoswich blocks viewed by 10*14 photomultiplier tubes (PMTs). The total number of crystals is 59,904×2=119,808. Each block has two scintillator layers, Lu_2SiO_5:Ce (LSO) and $Lu_{0.6}Y_{1.4}SiO_5$:Ce (LYSO) with an 8*8 crystal configuration per layer. The crystal size is 2.15*2.15*10 mm^3. The centre-to-centre distance between crystals is 2.4 mm. The axial field of view (FOV) is 25.2 cm, corresponding to 207 planes in the reconstructed images, with a pixel size of 1.218×1.218×1.218 mm^3 [1].

The spatial resolution of the system was measured in air with an ^{18}F point source positioned in the centre of the FOV and 10 cm off-centre. List mode data of the point source were reconstructed using the ordinary Poisson 3D ordered subset expectation maximization (OP-3D-OSEM) algorithm, with 6 iterations and 16 subsets. Data were reconstructed with the OP-3D-OSEM and not with analytical reconstruction according to the National Electrical Manufacturers Association (NEMA) standards.

More recently, image reconstruction has been performed on a Quad Core PC running a fast reconstruction algorithm developed by Hong et al. [12]. Based on the measurements performed by Sureau et al. [7], PSF modelling has recently been implemented within the fast reconstruction algorithm (the software was kindly provided by Dr. Merence Sibomana, Rigshopitalet, Copenhagen University Hospital, Denmark). The PSF model used in the fast reconstruction algorithm has been described in detail by Comtat et al. [13] in a multi-centre evaluation of the PSF reconstruction which also included our HRRT system. This PSF model differs from the model used by Sureau et al. [7] with regard to the projector used. In the regular HRRT reconstruction software for sinogram data the projector is based on a 3-D implementation of the Joseph's algorithm [14] and has a Gaussian shape. In the present approach an isotropic 3-D kernel was chosen for the OP-OSEM reconstruction algorithm with resolution modelling as described in Eq. 7 of Comtat et al. [13]. The PSF parameters used in the reconstruction were the default values of FWHM1=2.1 mm, FWHM2=5.9 mm, Gauss2/Gauss 1ratio=0.05. The PSF modelled in the reconstruction was isotropic and stationary. To measure resolution using PSF modelling, list mode data of the point source were also reconstructed using the advanced algorithm which includes resolution modelling of the PSF, with 10 iterations and 16 subsets (OP-3D-OSEM-PSF).

The NEMA IEC/2001 phantom

This is a phantom primarily used for assessment of the image quality of whole-body PET systems. The phantom consists of a large background compartment of approximately 6 l and 6 spheres of different diameter. The spheres and background can be filled with solutions having different radioactivity concentration. The diameters of the spheres were: 10, 13, 17, 22, 28 and 37 mm. Different concentrations were used in the spheres and different isotopes were used in the spheres and in the background since we aimed to simulate TACs in regions of different sizes, different radiotracer concentration and with different kinetic behaviour. In our experimental setting, the large sphere was filled with a solution of ^{18}F at a concentration of ~7 kBq/ml. The remaining spheres were filled with a solution of ^{18}F at a concentration of ~21 kBq/ml, whereas the background was filled with a solution of ^{11}C at a concentration of ~5–6 kBq/ml. A solution of ^{11}C was used for the background to simulate a low activity region having

lower signal to noise ratio than that of the spheres with different diameter. At the time of imaging the ratio of sphere to background concentration was measured in a well counter. The ratio for the 37-mm sphere was 1.4, whereas it was 4.3 for the remaining spheres.

The NEMA phantom was positioned in the HRRT and list mode data were acquired for 120 min. Images were reconstructed with 20 frames each having a duration of 6 min. A 6-min transmission scan with a rotating ^{137}Cs source was performed 12 h after the list mode acquisition to allow for physical decay of the radioisotopes.

Two reconstruction algorithms were applied: (1) OP-3D-OSEM with 6 iterations and 16 subsets and (2) OP-3D-OSEM-PSF, with 10 iterations and 16 subsets. The number of iterations was based on a previous observation that inclusion of resolution modelling with OP-3D-OSEM-PSF decreases the convergence rate of the algorithm [13]. However, to confirm the choice of the number of iterations for each algorithm data were also reconstructed using 10 iterations for the OP-3D-OSEM and 16 iterations for the OP-3D-OSEM-PSF. Images obtained with algorithm 1 will be referred to as native, while those obtained with algorithm 2 as PSF. Images were reconstructed without decay correction. Native images were also smoothed with a Gaussian filter of 2 mm FWHM for visual evaluation.

Volumes of interest (VOIs) were drawn on each sphere according to the inner diameter and then eroded by one pixel to reduce partial volume sampling. VOIs of the same size were copied to the background according to the NEMA standards [15]. The volumes of the VOIs for the series of spheres were: 0.2, 0.5, 1.5, 2.9, 7.3 and 16.9 cm^3.

TACs were obtained for the different spheres and for the background. The area under the curve (AUC) was calculated (kBq · ml^{-1} · min) as an estimate of the cumulative radioactivity concentration in each region.

For each of the spheres having the ratio to background equal to 4.3 (10- to 28-mm diameter), the contrast recovery coefficient CRC_{hot} was measured according to the following equation [15]:

$$CRC_{hot} = \frac{(C_{hot}/C_{bkg} - 1)}{(a_{hot}/a_{bkg} - 1)}$$

where C_{bkg} is the concentration in the background, C_{hot} is the concentration in the spheres, a_{hot} is the actual activity in spheres and a_{bkg} is the actual activity in the background. The ratio a_{hot} /a_{bkg} was measured in the well counter and decay corrected to the time of imaging. For simplicity, CRC_{hot} will be referred to as recovery coefficient (RC). For the calculation of C_{hot}/C_{bkg} TACs for each sphere and background were decay corrected to the start time of imaging and then the data of the first 75 min were averaged to remove possible bias due to low counting statistics in the background region [16].

To examine the different noise characteristics using either of the above approaches the standard deviation (SD) of the average radioactivity concentration in each VOI was taken as an estimate of the noise and plotted over time along with the mean value on native images, images smoothed with a Gaussian filter of 2 mm and on PSF images. To examine the effect of the number of iterations on the noise of native and PSF images, the coefficient of variance was calculated with different iteration number for each VOI.

The STEPBRAIN phantom

This STEreolithographed Phantom of the Brain (STEPBRAIN ©) is anthropomorphic and contains different fillable compartments for grey matter (GM) and white matter (WM) [17] (for a detailed description see http://lab.ibb.cnr.it/). The STEPBRAIN phantom was filled with [^{18}F]FDG in both compartments to obtain a GM to WM ratio of 7.9. This ratio was targeted to simulate a PET image of the benzodiazepine receptor ligand [^{11}C]flumazenil [18]. List mode acquisition of the phantom was performed for 60 min followed by a 6-min transmission scan. Images were reconstructed as described above for the NEMA phantom using algorithms 1 and 2.

To calculate the average radioactivity concentration in the GM and WM, binary masks of the two compartments were obtained by the segmentation of a computed tomography (CT) scan. To obtain the masks, the phantom was scanned in the 64 slice CT System Siemens Biograph (Siemens Molecular Imaging). The voxel size of the CT images was 0.39×0.39×5.0 mm. First, a CT scan of the empty phantom (CT-air) was performed to visualize the thickness of the walls. A new CT scan was performed when the GM compartment was filled with diluted contrast medium and the WM compartment with water, with approximately a ratio of 10 in Hounsfield units between GM and WM (CT). The CT was manually segmented in order to generate GM and WM masks, removing the contribution of the walls measured with the CT-air.

The GM and WM masks were used to measure the average radioactivity concentration in each compartment. For this analysis CT-air and CT were coregistered to PET images using a normalized mutual information algorithm in the software PMOD 2.85 (PMOD Group, Zurich, Switzerland). The same coregistration parameters were applied to the GM and WM masks. Figure 1 displays the CT-air, the CT and the GM and WM masks that all were coregistered to the PET images. In addition, VOIs were drawn in the centrum semiovale of both hemispheres to estimate the radiotracer concentration in a region where the PVE is considered to be negligible (Fig. 1).

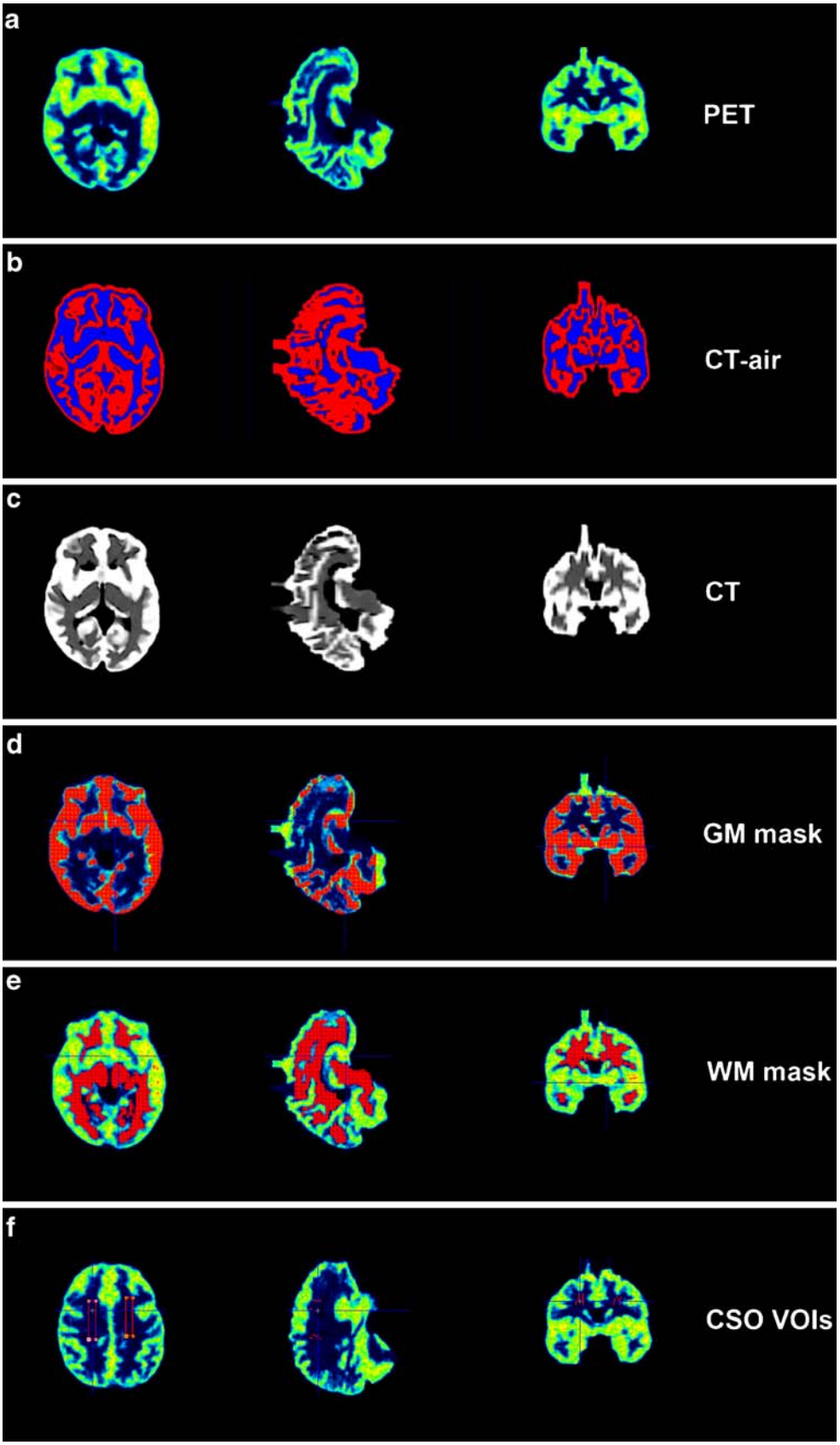

Fig. 1 Transaxial PET (**a**) and CT images (**b**, **c**) of the STEPBRAIN phantom at the level of the basal ganglia. Corresponding masks (**d**, **e**) for the grey matter (*GM*) and the white matter (*WM*) and small VOIs (**f**) at the level of the centrum semiovale (*CSO*)

Cynomolgus monkeys

Two female cynomolgus monkeys (housed at the Astrid Fagraeus Laboratory, SMI, Solna, Sweden) were included. The study was approved by the Animal Ethics Committee of the Swedish Animal Welfare Agency and was performed according to the "Guide for the Care and Use of Laboratory Animals" [19].

PET measurements were performed in the HRRT system. In the first monkey (6.5 kg) one PET measurement was conducted after intravenous injection of the dopamine transporter radioligand [^{18}F]FE-PE2I (67 MBq) [20]. Anaesthesia was induced and maintained by repeated intramuscular injections of a mixture of ketamine hydrochloride (3.75 mg/kg per h Ketalar®, Pfizer) and xylazine hydrochloride (1.5 mg/kg per h Rompun® Vet., Bayer). List mode data were acquired for 180 min and images were reconstructed with a series of 28 frames of increasing duration (60 s×5, 180 s×5, 360 s×5, 600 s×13).

In the second monkey (4.9 kg) one PET measurement was conducted after intravenous injection of the dopamine D_2 receptor radioligand [^{11}C]MNPA (197 MBq) [21]. Anaesthesia was induced by intramuscular injection of ketamine hydrochloride and maintained by a mixture of sevoflurane (2–6%) and air after endotracheal intubation. List mode data were acquired for 93 min. Images were reconstructed with a series of 28 frames of increasing duration (30 s×4, 60 s×4, 180 s×11, 360 s×9). In all PET measurements the head was immobilized with a fixation device [22]. Body temperature was maintained by Bair Hugger Model 505 (Arizant Healthcare Inc., Eden Prairie, MN, USA) and monitored by an oral thermometer. ECG, heart rate and respiratory rate were continuously monitored throughout the experiments. Blood pressure was monitored every 15 min.

Transmission scans were acquired for 6 min using a single ^{137}Cs source immediately before radioligand injection. Images were reconstructed using algorithms 1 and 2 described above. In monkey 1, VOIs were drawn for the caudate, putamen, midbrain and cerebellum on average images from 11 to 180 min using PMOD 2.85. In monkey 2, VOIs were drawn on the caudate, putamen and cerebellum for [^{11}C]MNPA. Delineation of VOIs was guided by an atlas of a cryosected cynomolgus monkey head [22].

Radioligand uptake was expressed as percent standardized uptake value (%SUV) and calculated as follows: Radioactivity concentration (kBq/cm^3) ÷ [injected activity (MBq) / body weight (kg)] ·100. TACs were obtained for each region and the AUC was calculated for each TAC as an estimate of the cumulative radioactivity concentration in each region. The binding potential (BP_{ND}) was estimated with the simplified reference tissue model (SRTM) [23] using the cerebellum as reference region. In the [^{18}F]FE-PE2I study, BP_{ND} was also estimated from native images reconstructed with 10 iterations and from PSF images reconstructed with 16 iterations. We selected [^{18}F]FE-PE2I for this purpose since this radioligand provides a quantifiable signal from brain regions with different transporter density, such as caudate, putamen and midbrain.

Human subject

One male control subject, 25 years old, underwent one PET measurement in the HRRT system with [^{11}C]raclopride (432 MBq), a reference radioligand for the D_2 dopamine receptor [24]. Before PET, a plaster helmet was made and used with a head fixation system during PET data acquisition as previously described [25]. The radioligand was administered as a bolus over 10 s and the IV line was immediately flushed with saline. A transmission scan was acquired for 6 min using a single ^{137}Cs source immediately before radioligand injection. List mode data were acquired for 63 min. Images were reconstructed with algorithms 1 and 2 with a series of 26 frames of increasing duration (15 s×4, 30 s×4, 60 s×6, 180 s×6, 360 s×6). PET images were coregistered with 3-D T1-weighted MRI data. ROIs were drawn on the caudate, putamen and cerebellum, using the Human Brain Atlas (HBA) software [26]. BP_{ND} was estimated with the SRTM using the cerebellum as reference region [23] from native images reconstructed with 6 and 10 iterations and from PSF images reconstructed with 10 and 16 iterations.

Results

The HRRT system

The in plane resolution with OP-3D-OSEM reconstruction was 2.3 mm FWHM in the centre of the FOV and 3.1 mm at 10 cm off-centre directions. The corresponding in plane resolution with OP-3D-OSEM-PSF was 1.5 mm FWHM in the centre of the FOV and 2.4 mm at 10 cm off-centre directions.

The NEMA IEC/2001 phantom

PSF reconstruction improved the visualization of the smallest spheres of the NEMA phantom as compared with native images (Fig. 2). TACs obtained from the spheres having a diameter between 10 and 28 mm showed that with PSF reconstruction the activity in all spheres was increased and the activity in the smallest spheres came closer to the spheres of large diameter (Fig. 2). The increase in AUC of the spheres with a diameter between 10 and 28 mm was inversely related to the diameter itself, ranging from 24.7% (10-mm diameter) to 4.6% (28-mm diameter). Even in the case of the largest sphere with 37-mm

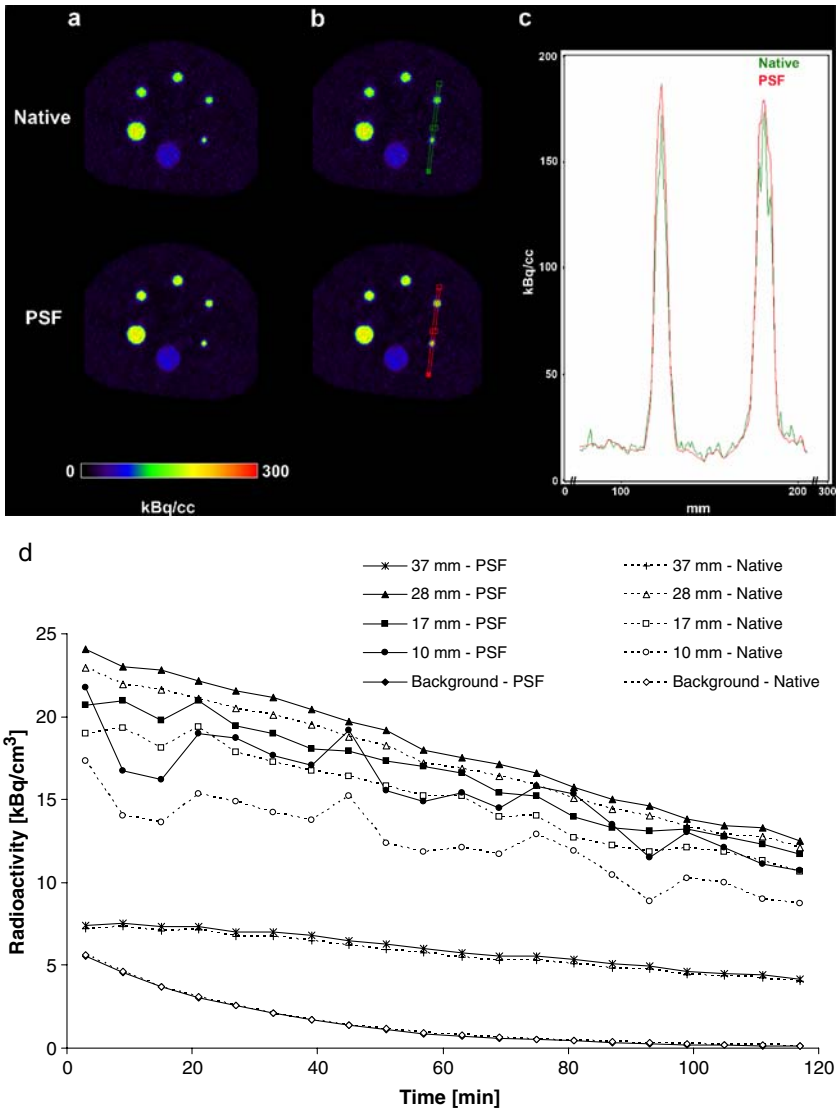

Fig. 2 **a** Transaxial PET images of the NEMA 2001 phantom. **b** The line profile drawn at the level of the two smallest spheres. **c** Corresponding plots of the line profile obtained from the reconstruction without (*native*) and with modelling of the point spread function (*PSF*). **d** TACs obtained from background and spheres of different diameter (10–37 mm) of the NEMA phantom. Note that the 37-mm sphere was filled with lower radioactivity

diameter the AUC increased by 4.2% using PSF reconstruction. Only a slight decrease (1.8%) in activity was observed in the background region with PSF reconstruction (Fig. 2).

The RC for the smallest sphere (10 mm) was 0.81 as compared to 0.58 for native images, while for the spheres having a diameter between 13 and 28 mm it was between 0.91 and 1.01 as compared to between 0.72 and 0.92 for native images (Table 1). The RC changed by 2% or less when the number of iterations was increased from 6 to 10 for the native images and from 10 to 16 for the PSF images (Table 1). The SD measured in each of the VOIs using PSF reconstruction was lower than in native images and came closer to the one measured in images smoothed with a Gaussian filter of 2 mm (Fig. 3a–c). The COV% for the VOIs of the background and of the spheres was higher in native images than in PSF images and increased with increasing number of iterations (Fig. 3d, e).

Table 1 Comparison of RC measured in spheres having a diameter from 10 to 28 mm using the two reconstruction algorithms, each with two different numbers of iterations

RC	10mm	13mm	17mm	22mm	28mm
Native, 6 iterations	0.58	0.72	0.76	0.87	0.92
Native, 10 iterations	0.56	0.71	0.75	0.86	0.92
PSF, 10 iterations	0.81	0.91	0.89	0.97	1.01
PSF, 16 iterations	0.83	0.91	0.88	0.96	1.00

The STEPBRAIN phantom

In the STEPBRAIN phantom, with PSF reconstruction the average GM radioactivity concentration increased by 4.4%, whereas the average WM radioactivity concentration decreased by 10.5% as compared with native images. This

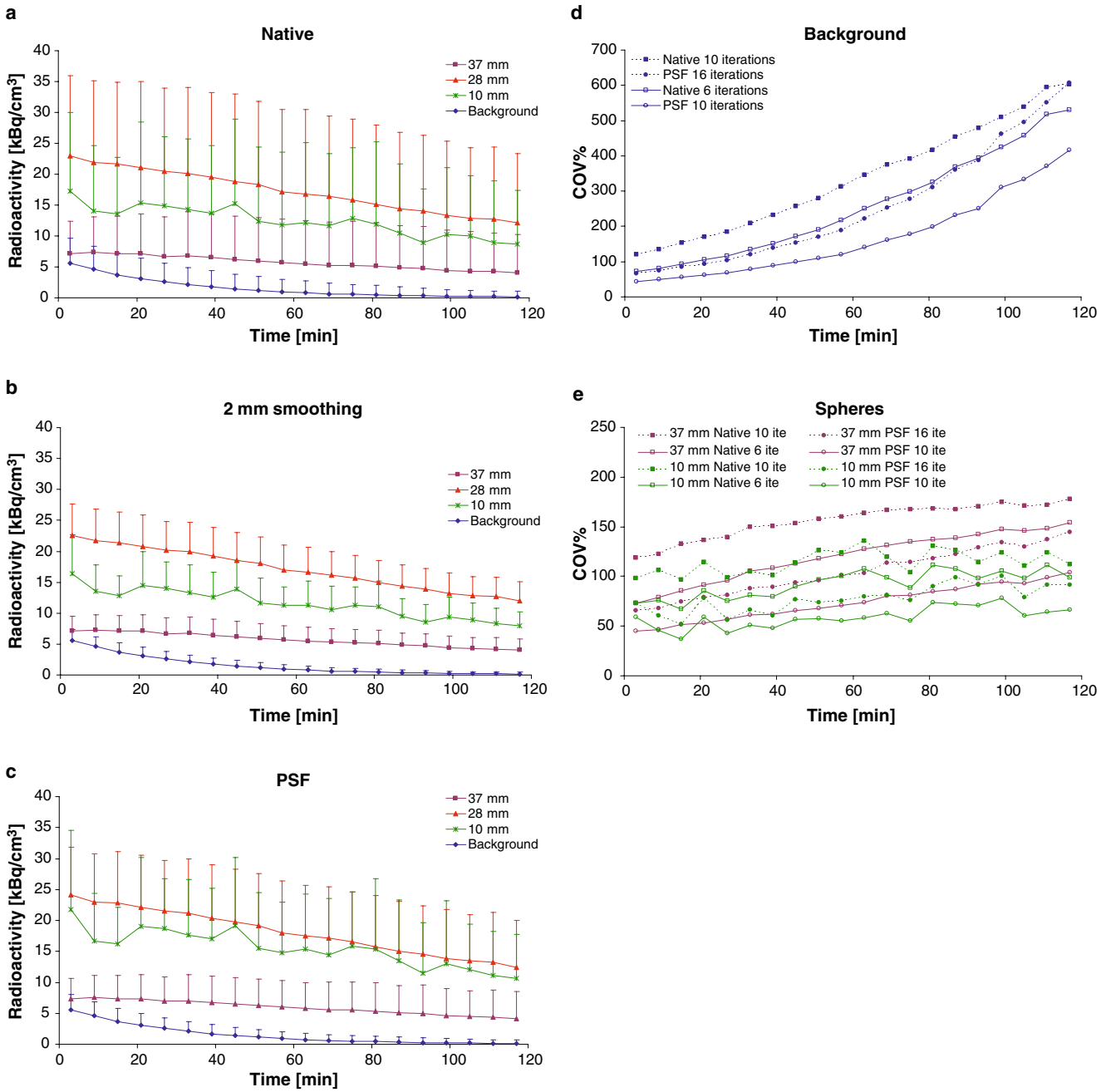

Fig. 3 TACs obtained from three representative spheres and from the background of the NEMA phantom showing the average radioactivity concentration plus one SD of each VOI as an indicator of the relative noise in the native image (**a**), the image smoothed with a Gaussian filter of 2 mm (**b**) and in the PSF image (**c**). Note that the 37-mm sphere was filled with lower radioactivity. The COV% in the VOIs of the background (**d**) and of two representative spheres (**e**) was plotted over time and as a function of the number of iterations

difference corresponds to a 17% increase of the GM to WM ratio with PSF reconstruction as compared with native images (percent of true ratio: 71 vs 61%, respectively). With PSF reconstruction the radioactivity concentration in the centrum semiovale decreased by 3.2%. When the centrum semiovale was used as WM region, 97% of the true GM to WM ratio was achieved with PSF reconstruction as compared with 90% of native images.

Cynomolgus monkeys

Visual inspection of [^{18}F]FE-PE2I images reconstructed with PSF showed better separation of caudate from putamen and better visualization of midbrain/substantia nigra as compared with native images (Fig. 4a). In PSF images the AUC of the TACs from the striatum and the midbrain were 16 and 14% higher than those measured in native images,

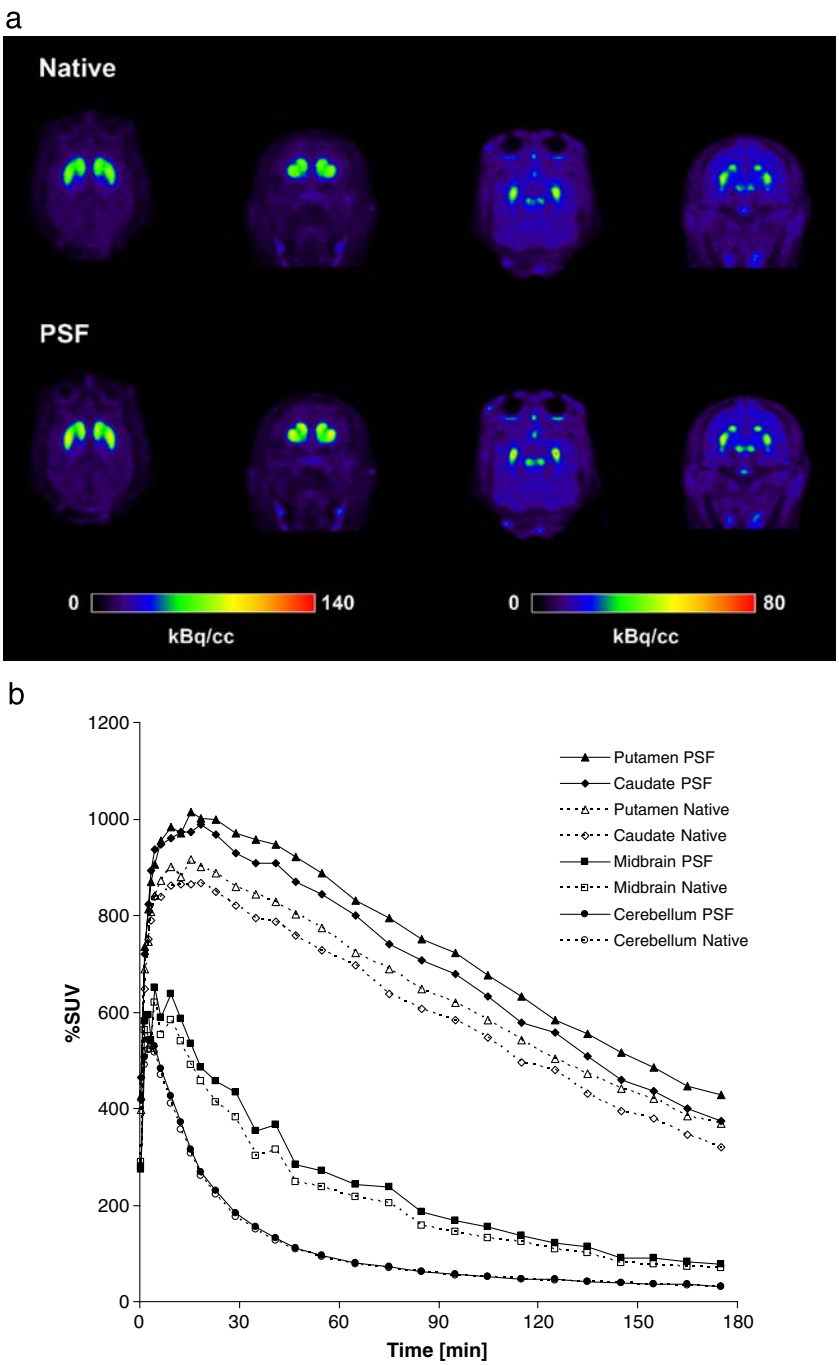

Fig. 4 **a** Transaxial (*first and third columns*) and coronal (*second and fourth columns*) HRRT PET images of [^{18}F]FE-PE2I binding in the same cynomolgus monkey obtained without and with PSF reconstruction. **b** TACs of [^{18}F]FE-PE2I binding in different brain regions obtained from native and PSF images

while the AUC of the cerebellum TAC was only 3% higher (Fig. 4b). PSF reconstruction increased BP_{ND} in the caudate and the putamen by 14% and in the midbrain by 18% (Table 2). In the native images the difference in BP_{ND} between 6 and 10 iterations was less than 2%, whereas in the PSF images the difference in BP_{ND} between 10 and 16 iterations was less than 5% (Table 2).

Image quality of the striatum was also improved by visual inspection of the PSF images of [^{11}C]MNPA (Fig. 5). The AUC of the TACs of [^{11}C]MNPA obtained from PSF reconstructed images were 9 and 8% higher than the native images in the caudate and the putamen and 6% higher in the cerebellum (Fig. 5). In the [^{11}C]MNPA study, using PSF reconstruction BP_{ND} increased by 6% in the caudate (from 1.54 to 1.63) and the putamen (from 1.47 and 1.55).

Human subject

Improved visualization of human striatum was also shown in [^{11}C]raclopride images obtained with PSF reconstruction

Table 2 Comparison of regional binding potential values for [^{18}F]FE-PE2I in a cynomolgus monkey using the two reconstruction algorithms, each with two different numbers of iterations

	Binding potential		
	Caudate	Putamen	Midbrain
Native, 6 iterations	5.52	6.03	1.01
Native, 10 iterations	5.50	6.02	1.03
PSF, 10 iterations	6.31	6.87	1.19
PSF, 16 iterations	6.32	6.90	1.25

and the AUC of the TACs from the caudate and the putamen were 9 and 6% higher than those obtained from the native images (Fig. 6). No difference was found in the cerebellum TAC when comparing native and PSF images. Using PSF reconstruction, BP_{ND} increased by 12% in the caudate and by 8% in the putamen (Table 3). In the native images the difference in BP_{ND} between 6 and 10 iterations was less than 2%, whereas in the PSF images the difference in BP_{ND} between 10 and 16 iterations was less than 3% (Table 3).

Discussion

This study was intended to further examine the implementation of PSF reconstruction in studies performed with the HRRT system. We applied the same approach of image reconstruction as previously reported by Sureau et al. [7] and used different experimental conditions to evaluate the effect of PSF reconstruction on quantitative parameters

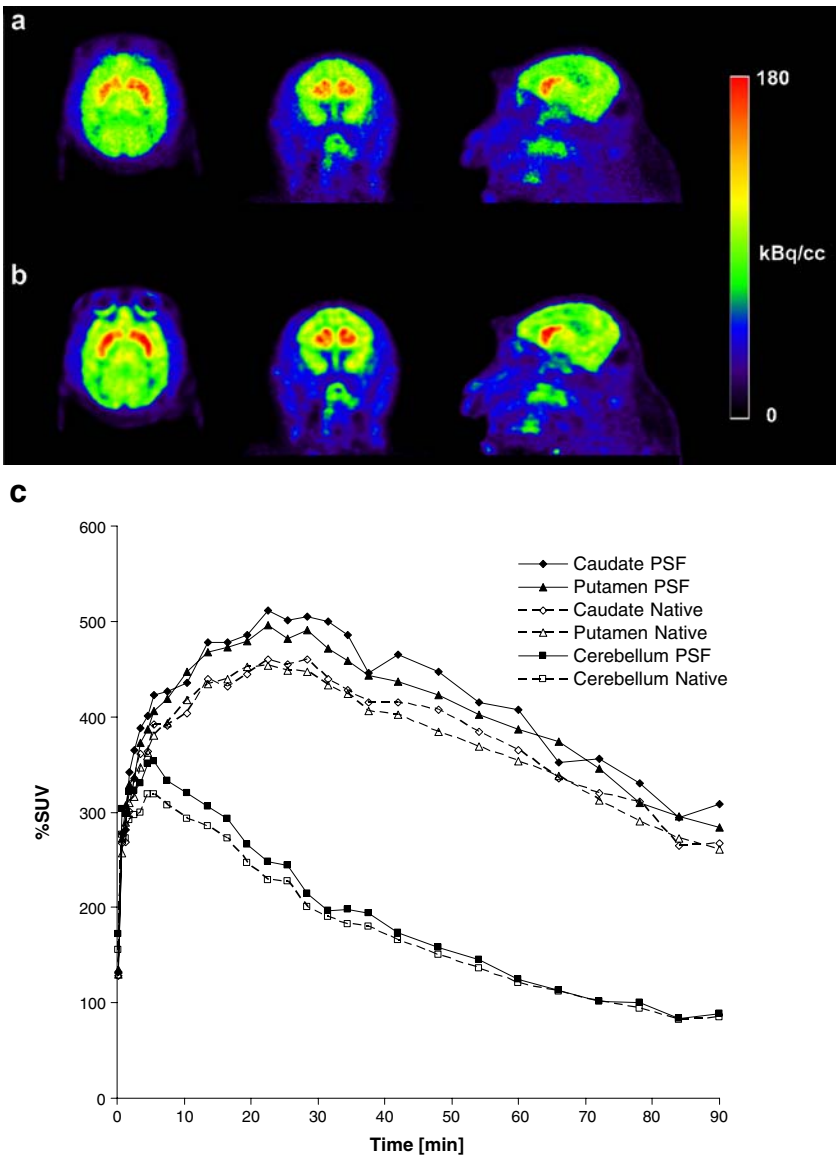

Fig. 5 PET images of [^{11}C] MNPA binding obtained in the same monkey without (**a**) and with (**b**) PSF reconstruction. **c** Corresponding regional TACs

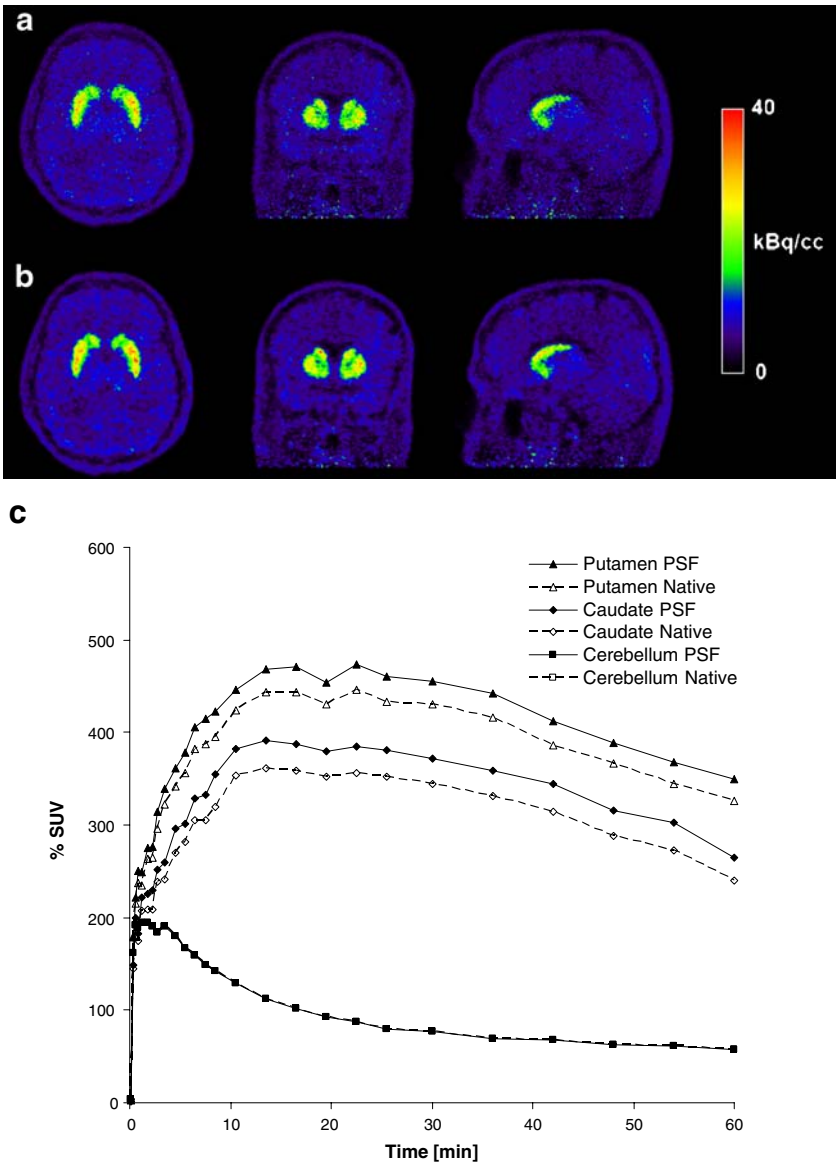

Fig. 6 PET images of [^{11}C] raclopride binding in a human subject obtained without (**a**) and with (**b**) PSF reconstruction. **c** Corresponding regional TACs

using different radioligands for the dopamine system. The study demonstrates that reconstruction using modelling of the PSF provides sizeable improvements of performance. The basis of such improvement relies on the improved image resolution obtained by compensation for the system's response function through modelling of the PSF in the reconstruction algorithm. The improved resolution translates into improved recovery and reduced PVE.

Table 3 Comparison of regional binding potential values for [^{11}C] raclopride in the human subject using the two reconstruction algorithms, each with two different numbers of iterations

	Binding potential	
	Caudate	Putamen
Native, 6 iterations	3.08	4.16
Native, 10 iterations	3.14	4.23
PSF, 10 iterations	3.45	4.48
PSF, 16 iterations	3.54	4.57

Improved recovery (RC) of the radioactivity concentration was demonstrated in the NEMA IEC/2001 phantom, in which PSF reconstruction yielded an RC of 0.81 for the smallest sphere of 10-mm diameter as opposed to an RC of 0.59 for native images. It has to be noted that in this study the purpose of the NEMA phantom was to simulate structures of different size and different kinetics between target and background. Therefore, it might be possible that the RC was slightly overestimated due to different physical properties (energy and positron range) of ^{18}F and ^{11}C. This difference would however not influence the results of the comparison between native and PSF images.

The visual examination of the line profiles across the different spheres and the TACs for the different regions examined showed that PSF reconstruction had larger impact on the radioactivity in the spheres than the background. With regard to the more uniform background radioactivity, this observation was in agreement with a previous report [7], also showing that PSF reconstruction decreases the variance among neighbouring voxels. In addition, the noise level of the VOIs for different spheres was lower in the PSF images than in the native images and came closer to the images smoothed with a Gaussian filter of 2 mm. Therefore, it appears that PSF reconstruction leads to an improvement in image resolution reducing also the noise in the image, as compared with the standard reconstruction using the OP-3D-OSEM.

The results in the STEPBRAIN phantom showed that PSF reconstruction reduces PVE and improves quantification of HRRT images. The line profiles across different sections of the phantom showed that the "spill-in" from the GM to WM was reduced in PSF images and the GM to WM ratio was increased. When the GM to WM ratio was calculated by using a small VOI at the level of the centrum semiovale, where PVE is negligible, the ratio was close to 100% of the true ratio, further confirming that PSF reconstruction improves the accuracy of the quantification.

The results in the cynomolgus monkeys and in the human subject showed that PSF reconstruction increases the BP_{ND} values mainly by an effect on the measured radioactivity concentration in the target region, whereas the effect was smaller in the reference region. This differential effect appears to be related to the behaviour of the radioligand used. In the case of [^{18}F]FE-PE2I, the increase of BP_{ND} was 14% in the striatum and 18% in the midbrain, while for [^{11}C]MNPA the increase of BP_{ND} was approximately 6%. In the cynomolgus monkey [^{18}F]FE-PE2I has a higher target to background ratio than [^{11}C]MNPA. A possible explanation is that the spill-over effect from ROIs in high contrast images may be more pronounced than in low contrast images resulting in lower recovery. When reference tissue models are applied the improvement in quantification using PSF reconstruction might thus be higher for those radioligands with high specific to non-displaceable binding ratio (i.e. [^{11}C]PE2I).

With regard to the human PET measurement with [^{11}C] raclopride, the increase in BP_{ND} using PSF reconstruction was approximately 10%. This increase was lower than the improvement previously reported for [^{11}C]PE2I [7], which has a higher target to background ratio than [^{11}C]raclopride, suggesting again that the improvement in quantification using PSF reconstruction is directly related to better contrast recovery in the images.

The results from the NEMA IEC/2001 phantom as well as the [^{18}F]FE-PE2I and the [^{11}C]raclopride studies suggest that only a marginal improvement in the outcome measures is achieved by increasing the number of iterations. In addition, a sizeable increase in the noise level of the images was evident in native and PSF images reconstructed with 10 or 16 iterations, respectively. Therefore, we considered that for PSF reconstruction 10 iterations should be sufficient to reach convergence in different regions at various experimental conditions.

Several methods based on segmentation of MR images are currently available for PVE correction [8, 10, 11] and implemented in applied studies with different PET radioligands [27, 28]. However, PVE correction methods based on MR segmentation assume homogeneous uptake in each of the segmented regions, which might not be appropriate for each biological condition. In addition, brain structures such as the midbrain or the brainstem, containing small regions or nuclei such as the substantia nigra or the locus coeruleus, cannot be segmented by standard MRI sequences and acceptable post hoc methods for PVE correction are not available. Therefore, PSF reconstruction appears to reduce the need for sizeable PVE corrections in such regions. Along with PVE, head motion is another important factor limiting image resolution, particularly for the HRRT system. In this study, the head fixation systems used for non-human primates and the human subject were designed to minimize head motion in the PET system. Methods of correction for head motion are currently under investigation and might become more widely available in the future. The contribution of head motion to the spatial resolution of the images and the accuracy of quantification requires further evaluation, which was beyond the scope of this study.

Conclusion

This study provides further support for the suggestion that PSF reconstruction of PET images improves neuroreceptor quantification by improving the image resolution and reducing PVE. In combination with the high resolution of the HRRT system, this approach provides improved conditions for applied studies of psychiatric and neurodegenerative disorders, in particular when receptor populations in small brain structures are examined.

Acknowledgments The authors would like to thank members of the Karolinska Institutet PET Centre for assistance in the PET experiments. The authors also thank Drs. Inki Hong and Merence Sibomana for implementation of the PSF modelling in the fast reconstruction software, and Dr. Bruno Alfano for providing the STEPBRAIN phantom.

This study was presented in abstract form at the Neuroreceptor Mapping 2008 Meeting, Pittsburgh, PA, USA, and at the European Association of Nuclear Medicine 2008 Congress, Munich, Germany. This study was funded in part by the EC - FP6-project DiMI, LSHB-CT-2005-512146 and by VR Swedish Science Council 48105.

References

1. de Jong HW, van Velden FH, Kloet RW, Buijs FL, Boellaard R, Lammertsma AA. Performance evaluation of the ECAT HRRT: an LSO-LYSO double layer high resolution, high sensitivity scanner. Phys Med Biol 2007;52:1505–26. doi:10.1088/0031-9155/52/5/019.
2. Heiss WD, Habedank B, Klein JC, Herholz K, Wienhard K, Lenox M, et al. Metabolic rates in small brain nuclei determined by high-resolution PET. J Nucl Med 2004;45:1811–5.
3. Horti AG, Fan H, Kuwabara H, Hilton J, Ravert HT, Holt DP, et al. 11C-JHU75528: a radiotracer for PET imaging of CB1 cannabinoid receptors. J Nucl Med 2006;47:1689–96.
4. Leroy C, Comtat C, Trébossen R, Syrota A, Martinot JL, Ribeiro MJ. Assessment of 11C-PE2I binding to the neuronal dopamine transporter in humans with the high-spatial-resolution PET scanner HRRT. J Nucl Med 2007;48:538–46. doi:10.2967/jnumed.106.037283.
5. Hirvonen J, Johansson J, Teräs M, Oikonen V, Lumme V, Virsu P, et al. Measurement of striatal and extrastriatal dopamine transporter binding with high-resolution PET and [(11) C]PE2I: quantitative modeling and test-retest reproducibility. J Cereb Blood Flow Metab 2008;28:1059–69. doi:10.1038/sj.jcbfm.9600607.
6. Panin VY, Kehren F, Michel C, Casey M. Fully 3-D PET reconstruction with system matrix derived from point source measurements. IEEE Trans Med Imaging 2006;25:907–21. doi:10.1109/TMI.2006.876171.
7. Sureau FC, Reader AJ, Comtat C, Leroy C, Ribeiro MJ, Buvat I, et al. Impact of image-space resolution modeling for studies with the high-resolution research tomograph. J Nucl Med 2008;49:1000–8. doi:10.2967/jnumed.107.045351.
8. Quarantelli M, Berkouk K, Prinster A, Landeau B, Svarer C, Balkay L, et al. Integrated software for the analysis of brain PET/SPECT studies with partial-volume-effect correction. J Nucl Med 2004;45:192–201.
9. Rousset OG, Ma Y, Evans AC. Correction for partial volume effects in PET: principle and validation. J Nucl Med 1998;39:904–11.
10. Rousset OG, Deep P, Kuwabara H, Evans AC, Gjedde AH, Cumming P. Effect of partial volume correction on estimates of the influx and cerebral metabolism of 6-[(18) F]fluoro-L-dopa studied with PET in normal control and Parkinson's disease subjects. Synapse 2000;37:81–9. doi:10.1002/1098-2396(200008)37:2<81::AID-SYN1>3.0.CO;2-#.
11. Müller-Gärtner HW, Links JM, Prince JL, Bryan RN, McVeigh E, Leal JP, et al. Measurement of radiotracer concentration in brain gray matter using positron emission tomography: MRI-based correction for partial volume effects. J Cereb Blood Flow Metab 1992;12:571–83.
12. Hong IK, Chung ST, Kim HK, Kim YB, Son YD, Cho ZH. Ultra fast symmetry and SIMD-based projection-backprojection (SSP) algorithm for 3-D PET image reconstruction. IEEE Trans Med Imaging 2007;26:789–803. doi:10.1109/TMI.2007.892644.
13. Comtat C, Sureau FC, Sibomana M, Hong IK, Sjöholm N, Trébossen R. Image based resolution modeling for the HRRT OSEM reconstructions software. Paper presented at: IEEE Nuclear Science Symposium Conference Record, 2008; Dresden, Germany.
14. Joseph PM. An improved algorithm for reprojecting rays through pixel images. IEEE Trans Med Imaging 1982;1:192–6. doi:10.1109/TMI.1982.4307572.
15. Daube-Witherspoon ME, Karp JS, Casey ME, DiFilippo FP, Hines H, Muehllehner G, et al. PET performance measurements using the NEMA NU 2–2001 standard. J Nucl Med 2002;43:1398–409.
16. Reilhac A, Tomeï S, Buvat I, Michel C, Keheren F, Costes N. Simulation-based evaluation of OSEM iterative reconstruction methods in dynamic brain PET studies. Neuroimage 2008;39:359–68. doi:10.1016/j.neuroimage.2007.07.038.
17. Alfano B, Prinster A, Quarantelli M, Brunetti A, Salvatore M. STEPBRAIN: A stereolitographed phantom of the brain for nuclear medicine, computed tomography, and magnetic resonance applications. Paper presented at: RSNA, 2003.
18. Odano I, Halldin C, Karlsson P, Varrone A, Airaksinen AJ, Krasikova RN, et al. [(18)F]Flumazenil binding to central benzodiazepine receptor studies by PET—quantitative analysis and comparisons with [(11)C]flumazenil. Neuroimage 2009;45:891–902.
19. Clark JD, Gebhart GF, Gonder JC, Keeling ME, Kohn DF. Special Report: The 1996 Guide for the Care and Use of Laboratory Animals. ILAR J 1997;38:41–8.
20. Varrone A, Steiger C, Schou M, Takano A, Finnema SJ, Guilloteau D, et al. In vitro autoradiography and in vivo evaluation in cynomolgus monkey of [18F]FE-PE2I, a new dopamine transporter PET radioligand. Synapse. 2009; In press.
21. Finnema SJ, Seneca N, Farde L, Shchukin E, Sóvágó J, Gulyás B, et al. A preliminary PET evaluation of the new dopamine D2 receptor agonist [11C]MNPA in cynomolgus monkey. Nucl Med Biol 2005;32:353–60. doi:10.1016/j.nucmedbio.2005.01.007.
22. Karlsson P, Farde L, Halldin C, Swahn CG, Sedvall G, Foged C, et al. PET examination of [11C]NNC 687 and [11C]NNC 756 as new radioligands for the D1-dopamine receptor. Psychopharmacology (Berl) 1993;113:149–56. doi:10.1007/BF02245691.
23. Lammertsma AA, Hume SP. Simplified reference tissue model for PET receptor studies. Neuroimage 1996;4:153–8. doi:10.1006/nimg.1996.0066.
24. Farde L, Hall H, Ehrin E, Sedvall G. Quantitative analysis of D2 dopamine receptor binding in the living human brain by PET. Science 1986;231:258–61. doi:10.1126/science.2867601.
25. Bergström M, Boëthius J, Eriksson L, Greitz T, Ribbe T, Widén L. Head fixation device for reproducible position alignment in transmission CT and positron emission tomography. J Comput Assist Tomogr 1981;5:136–41. doi:10.1097/00004728-198102000-00027.
26. Roland PE, Graufelds CJ, Wahlin J, Ingelman L, Andersson M, Ledberg A, et al. Human brain atlas: for high-resolution functional and anatomical mapping. Hum Brain Mapp 1994;1:173–84. doi:10.1002/hbm.460010303.
27. Giovacchini G, Toczek MT, Bonwetsch R, Bagic A, Lang L, Fraser C, et al. 5-HT 1A receptors are reduced in temporal lobe epilepsy after partial-volume correction. J Nucl Med 2005;46:1128–35.
28. Hasselbalch SG, Madsen K, Svarer C, Pinborg LH, Holm S, Paulson OB, et al. Reduced 5-HT2A receptor binding in patients with mild cognitive impairment. Neurobiol Aging 2008;29:1830–8. doi:10.1016/j.neurobiolaging.2007.04.011.